

The KiTS19 Challenge Data: 300 Kidney Tumor Cases with Clinical Context, CT Semantic Segmentations, and Surgical Outcomes

Nicholas Heller¹, Niranjan Sathianathan¹, Arveen Kalapara¹, Edward Walczak¹, Keenan Moore², Heather Kaluzniak³, Joel Rosenberg¹, Paul Blake¹, Zachary Rengel¹, Makinna Oestreich¹, Joshua Dean¹, Michael Tradewell¹, Aneri Shah¹, Resha Tejpaal¹, Zachary Edgerton¹, Matthew Peterson¹, Shaneabbas Raza³, Subodh Regmi¹, Nikolaos Papanikolopoulos¹, and Christopher Weight¹

¹ University of Minnesota

² Carleton College

³ University of North Dakota

{helle246, cjweight}@umn.edu

Abstract. The morphometry of a kidney tumor revealed by contrast-enhanced Computed Tomography (CT) imaging is an important factor in clinical decision making surrounding the lesion’s diagnosis and treatment. Quantitative study of the relationship between kidney tumor morphology and clinical outcomes is difficult due to data scarcity and the laborious nature of manually quantifying imaging predictors. Automatic semantic segmentation of kidneys and kidney tumors is a promising tool towards automatically quantifying a wide array of morphometric features, but no sizeable annotated dataset is currently available to train models for this task. We present the KiTS19 challenge dataset: A collection of multi-phase CT imaging, segmentation masks, and comprehensive clinical outcomes for 300 patients who underwent nephrectomy for kidney tumors at our center between 2010 and 2018. 210 (70%) of these patients were selected at random as the training set for the 2019 MICCAI KiTS Kidney Tumor Segmentation Challenge and have been released publicly. With the presence of clinical context and surgical outcomes, this data can serve not only for benchmarking semantic segmentation models, but also for developing and studying biomarkers which make use of the imaging and semantic segmentation masks.

Keywords: Kidney Tumors · Nephrometry · Semantic Segmentation

1 Background

There were more than 400,000 kidney cancer diagnoses worldwide in 2018 resulting in more than 175,000 deaths [1], up from 208,000 diagnoses and 102,000

deaths in 2002 [19]. The incidence is higher in developed countries than in developing countries, and peaks between the ages of 60 and 70 [2]. With the proliferation of abdominal imaging for various unrelated indications, the incidental detection of asymptomatic renal masses has become increasingly common. This has increased the proportion of tumors that are small and localized when treated, which is thought to be a contributing factor to the disease’s increased overall survival [10]. Some established risk factors for kidney cancer are cigarette smoking, obesity, and hypertension [3]. Historically, removal of both the tumor and affected kidney, termed Radical Nephrectomy (RN), was standard of care for kidney tumors, but advancements in surgery in conjunction with earlier tumor detection have precipitated a significant shift in kidney cancer treatment toward more conservative nephron sparing procedures, termed Partial Nephrectomies (PNs) [21]. These are typically less invasive and limit renal function impairment, thus they are preferred when feasible.

In an effort to more reliably quantify tumor details and accurately compare decisions about kidney tumor treatment (notably, the decision between RN and PN), various *nephrometry* scoring systems were proposed based on the tumor’s presentation in cross-sectional imaging. Among these are R.E.N.A.L. [13], P.A.D.U.A. [6], and the Centrality Index [20]. Once proposed, these scoring systems were found to be associated with surgical approach and a wide range of clinical outcomes including recurrence after treatment [17,7], benign vs malignant tumor [18], and high-grade tumor pathology [12]. In spite of their impressive predictive power, existing nephrometry scores characteristically utilize relatively simple and easy-to-extract image features such as location, degree of endophycity, and diameter of the tumor. Further, the most popular R.E.N.A.L. and P.A.D.U.A. scores reduce continuous variables into discrete bins, further limiting their expressive power in favor of more expedient and repeatable manual evaluation [11]. In contrast, semantic segmentation produces a rich quantitative representation of the tumor and affected organ, trivializing the precise extraction of enumerable morphological traits such as contact surface area [15] and irregularity [22].

Our objectives in releasing this data are (1) to accelerate the research and development of new nephrometric features to aid in prognosis and treatment planning for kidney tumors, and (2) to enable the creation of reliable learning-based kidney and kidney tumor semantic segmentation methods which will allow the features developed in (1) to be automated and applied at an unprecedented scale.

2 Methods

We conducted a retrospective review⁴ of the 544 patients who underwent RN or PN at our institution between 2010 and mid-2018 to excise a renal tumor. For 326 of these patients, preoperative abdominal CT imaging in the late-arterial

⁴ This work was reviewed and approved by the Institutional Review Board at the University of Minnesota.

phase was available, and the remaining patients were excluded. To simplify an unambiguous definition of kidney tumor voxels, all patients with tumor thrombus were also excluded, leaving 300 patients who met our inclusion criteria and comprise our dataset.

The data collection procedure for each patient who met our inclusion criteria consisted of four steps: (1) chart review, (2) CT collection, (3) CT annotation, and (4) quality assurance. This work was done primarily by students under the supervision of author Christopher Weight, an experienced fellowship-trained urologic oncologist who specializes in kidney tumors.

2.1 Chart Review

The objective of the chart review phase of the data collection procedure was to record relevant clinical information about each patient’s demographics, comorbidities, intervention, and clinical outcomes. This information was found by a manual review of each patient’s Electronic Medical Record (EMR) in conjunction with a database query for certain structured fields. An exhaustive list and short description of each of the collected attributes from this phase can be found in Section 3.

2.2 CT Collection

The objective of the CT collection phase of the data collection procedure was to secure a local copy of the most recent preoperative CT study for each patient that contained at least one series in late arterial contrast phase that depicts the entirety of the abdomen (at least). Such imaging is standard of care for kidney tumors [2], but many patients were excluded at this stage not because they hadn’t undergone this imaging, but rather because it was either done at a referring institution and not available to us for download, or MRI was used for preoperative planning.

In rare cases where several preoperative studies captured within one week of each other meet this criteria, preference was given to the study containing the late arterial series with smallest slice-thickness.

2.3 CT Annotation

Once a patient’s clinical attributes and imaging were collected, they were moved to the third phase of our data collection procedure: manual delineation of the kidney and tumor boundaries. To perform these annotations in a distributed manner, we developed a simple web application based on the HTML5 *Canvas* element that allowed users to draw freehand contours on images [9]. All annotations were performed in the transverse plane, and series were regularly subsampled in the longitudinal direction such that the number of annotated slices depicting any kidney was roughly 50 per patient. Interpolation (described later) was performed to compute labels for the excluded slices.

Manual Delineation The students performing these annotations were given the following instructions:

1. Confirm that the collection of images for this patient depicts the entirety of all kidneys. Some of the patients found in our review had horseshoe kidneys or were transplant recipients. These were included so long as the vast majority of all kidneys were shown. Let the i th case have J transverse slices. We will refer to the voxels from the j th slice of the i th case as $I_j^{(i)}$.
2. For each connected component of pixels belonging to a region of interest, draw a contour which *includes* the entire renal capsule and any renal tumors or cysts, but *excludes* all tissue other than renal parenchyma that appears more radiodense than the perinephric fat. In slices where the hilum was present, the students were to introduce a concavity so as to exclude the bright ureter and renal vessels (see Fig. 1b). Let there be $N_j^{(i)}$ such contours in the j th axial section of the i th case. We will refer to the set of voxels inside one of these contours by $A_{j,n}^{(i)}$.
3. For each connected component of tumor tissue, draw a contour which *includes* that tumor component, but *excludes* all kidney tissue. Effectively, these contours only specify the interface between the kidney and tumor, since the rest of the tumor boundary was already specified in step 2 (see Fig. 1c). Let there be $M_j^{(i)}$ such contours in the j th image of the i th case. We will refer to the set of voxels inside one of these contours by $C_{j,m}^{(i)}$.

This annotation procedure enabled the students to provide a complete and unambiguous representation of the kidneys and kidney-tumor boundary while limiting the number of tedious, voxel-wise decisions.

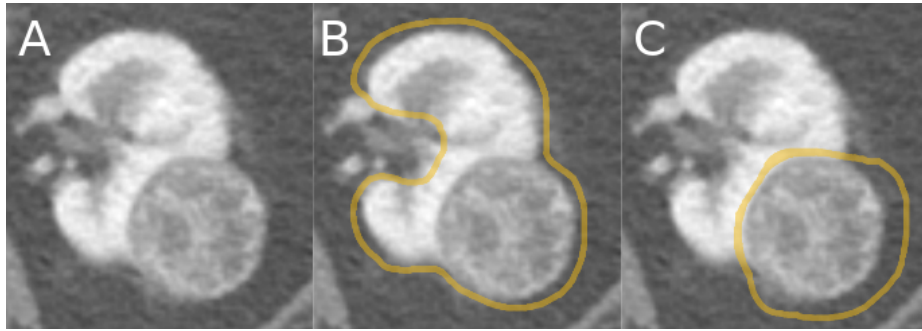


Fig. 1. Left: An axial section of a kidney and tumor from the database, $I_j^{(i)}$. **Middle:** An example of the first contour the students were instructed to draw around the whole renal capsule and tumor but excluding the intra-hilar structures, $\partial A_{j,0}^{(i)}$. **Right:** An example of the second contour the students were instructed to draw which includes the tumor but excludes all kidney tissue, $\partial C_{j,0}^{(i)}$.

Thresholding and Hilum Filling It is well-established that kidneys, tumors, and cysts ($\text{HU} > 0.0$) are significantly more radiodense than fat ($\text{HU} < -90.0$) [14], thus a simple HU threshold can be used to precisely define the boundary between the two. Certain CT series, those especially captured with low-dose techniques [16], exhibit random noise which can degrade the performance of the threshold-defined boundary. To mitigate this, we convolve a 3x3 mean filter with each slice before performing a threshold. Experimentally, we determined that a cutoff of -30.0 HU successfully discriminated perinephric fat and the tissue in our regions of interest. In certain cases where the CT had a large amount of noise and no cysts were present, we applied a 7x7 median filter to each slice and raised the threshold value to 0 HU. We will refer to the set voxels in the j th slice of the i th case found to be above its respective threshold as $S_j^{(i)}$.

Between the manually-drawn contours and the thresholding, we partition the voxels from our annotated slices into three bins:

1. Loose Background, B_{loose} , a superset of True Background B , everything outside of the intersection between the thresholded voxels, $S_j^{(i)}$ and the union of all kidney+tumor contour interiors, $A_j^{(i)}$

$$B_j^{(i)} \subseteq B_{loose,j}^{(i)} = I_j^{(i)} \setminus \left(\bigcup_{m=1}^{M_j^{(i)}} A_{j,m}^{(i)} \cap S_j^{(i)} \right)$$

2. True Tumor, T , the intersection of the tumor contour interiors, $C_j^{(i)}$, with the kidney contour interiors, $A_j^{(i)}$, and threshold, $S_j^{(i)}$

$$T_j^{(i)} = \left(\bigcup_{m=1}^{M_j^{(i)}} A_{j,m}^{(i)} \cap S_j^{(i)} \right) \cap \left(\bigcup_{n=1}^{N_j^{(i)}} C_{j,n}^{(i)} \right)$$

3. Strict Kidney, K_{strict} , a subset of true kidney, K , voxels which appear in the intersection of the kidney contour interiors and threshold but not the tumor contour interiors.

$$K_j^{(i)} \supseteq K_{strict,j}^{(i)} = \left(\bigcup_{m=1}^{M_j^{(i)}} A_{j,m}^{(i)} \cap S_j^{(i)} \right) \cap \left(\bigcap_{n=1}^{N_j^{(i)}} I_j^{(i)} \setminus C_{j,n}^{(i)} \right)$$

These bins are depicted in Fig. 2b. Consider the kidney or cyst voxels excluded from K_{strict} . We refer to these as $K_{exc,j}^{(i)} = K_j^{(i)} \setminus K_{strict,j}^{(i)}$. By definition:

$$\begin{aligned} K_j^{(i)} &= K_{strict,j}^{(i)} \cup K_{exc,j}^{(i)} \\ B_j^{(i)} &= B_{loose,j}^{(i)} \setminus K_{exc,j}^{(i)} \end{aligned}$$

Therefore, if we identify K_{exc} , we can compute the final ground truth partition, B , K , and T for each annotated slice.

On inspection and trial we found that reliably delineating the boundary between the complex intra-hilar structures and kidney parenchyma is not feasible, and to attempt this would only introduce ambiguity and error into our dataset, something that’s been shown to markedly hinder the performance of deep learning-based automatic segmentation [8].

To address this, we chose to include these intra-hilar structures in our ”kidney” label. We define the boundary for these features to be that line which spans the concavity formed by the exclusion of this tissue in the manually-drawn contours (see Fig. 2b). This line, $H_j^{(i)}$, is computed by a call to OpenCV’s `convexHull()` function followed by `convexityDefects()`. An heuristic approach based on location and shape was used to automatically select the correct defect, but in cases where visual inspection showed that it failed, the line selection was manually corrected. Thus, $K_j^{(i)}$ is defined by the inclusive interior of the contour given by $\partial K_{strict,j}^{(i)} \cup H_j^{(i)}$, where ∂K denotes the set K ’s boundary.

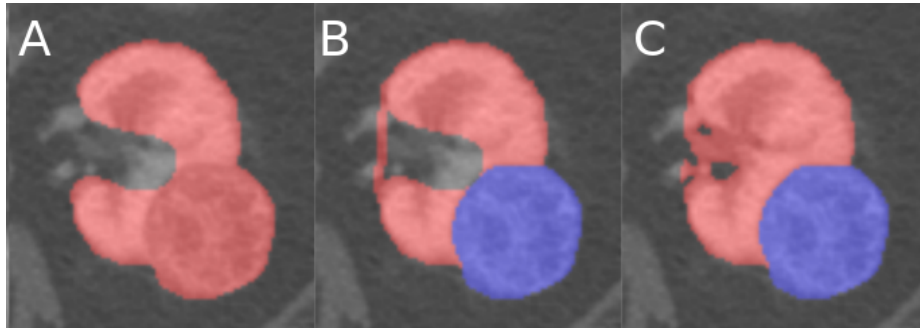


Fig. 2. A demonstration of the various stages of the algorithm which produces the ground truth segmentation masks given the manually-drawn contours, best viewed in color. **Left:** The union of all the strict kidney sets, $K_{strict,j}^{(i)}$. **Middle:** The hilum found by the heuristic based detection algorithm as well as the true tumor found by the intersection of the tumor contour with the left figure, $K_{strict,j}^{(i)} \cup H_j^{(i)}$. **Right:** The final kidney and tumor labels found by including all tissue within the hilum that’s above the threshold, blue: $T_j^{(i)}$, red: $K_j^{(i)}$.

Interpolation Until now, we have described only the procedure defining the ground truth given these manually drawn contours, but for practical reasons only a fraction of the total number of slices containing a region of interest were annotated. In order to produce contours for the remaining slices, and interpolation methodology was used. Our algorithm for interpolating contours for the l th slice from contours drawn in slices $l + a$ and $l - b$ in Algorithm 1. Once these

contours are inferred, the ground truth is computed just as it is for manually provided contours.

Algorithm 1 Interpolate Contours

```

1: function MATCHCONTOURPOINTS(contour1, contour2)
2:   result  $\leftarrow$  []
3:   for  $\mathbf{x}$  in contour1 do
4:     mindist  $\leftarrow inf$ 
5:      $\mathbf{m} \leftarrow$  Centroid(contour1)
6:     for  $\mathbf{y}$  in contour2 do
7:       if  $\|\mathbf{x} - \mathbf{y}\|_2 < mindist$  then
8:         mindist  $\leftarrow \|\mathbf{x} - \mathbf{y}\|_2$ 
9:          $\mathbf{m} \leftarrow \mathbf{y}$ 
10:    Append( $(\mathbf{x}, \mathbf{m})$ , result)
11:  return result
12: # Populates  $A_l^{(i)}$ ,  $C_l^{(i)}$ , W.L.O.G Assume  $M_{l+a}^{(i)} \geq M_{l-a}^{(i)}$ ,  $N_{l+a}^{(i)} \geq N_{l-a}^{(i)}$ 
13:  $D_{max} \leftarrow 20$  # Maximum distance where contours are still morphed together
14:  $A_l^{(i)} \leftarrow \{\}$ 
15: for  $m$  in  $\{1 \dots M_{l+a}^{(i)}\}$  do
16:    $P \leftarrow$  nearest of contours from  $A_{l-b}^{(i)}$  or  $\{\}$  if nearest is farther than  $D_{max}$ 
17:    $R \leftarrow$  MatchContourPoints( $A_{l-b,m}^{(i)}$ ,  $P$ )
18:    $A_l^{(i)} \leftarrow A_l^{(i)} \cup \left\{ \frac{a}{a+b} * R[:, 1] + \frac{b}{a+b} * R[:, 2] \right\}$ 
19: for  $n$  in  $\{1 \dots N_{l+a}^{(i)}\}$  do
20:    $P \leftarrow$  nearest of contours from  $C_{l-b}^{(i)}$  or  $\{\}$  if nearest is farther than  $D_{max}$ 
21:    $R \leftarrow$  MatchContourPoints( $C_{l-b,n}^{(i)}$ ,  $P$ )
22:    $C_l^{(i)} \leftarrow C_l^{(i)} \cup \left\{ \frac{a}{a+b} * R[:, 1] + \frac{b}{a+b} * R[:, 2] \right\}$ 

```

2.4 Quality Assurance

Chart Review During chart review, the students were instructed to leave blank any field that they were not certain about. These fields were then revisited at a later time by two students. If those students did not agree on the field’s correct value, author Christopher Weight was consulted to make the final determination.

Imaging Annotations Students performing annotations were instructed to read the radiology note from the preoperative CT scan in order to properly locate and delineate the tumor(s) in concordance with the expert clinician. A reviewing student examined each and every image-ground truth pair in both the transverse and coronal planes, checking for consistent boundary treatment, and once again for concordance with the radiologist’s impression. Cases found

to have minor issues were fixed by this reviewing student directly, and then accepted, whereas rare cases with major issues were sent back to the first student for fixing, and subsequent re-review. This second practice helped to not only reduce the annotation burden on the reviewing student, but also to educate the annotating students and prevent similar issues in the future. We discuss our method's interobserver variability in section 4.

3 Data Records

In its original form, the KiTS dataset has a single JSON file, `kits.json`, along with a directory, `data/` with a subdirectory for each case containing its large binary objects. `kits.json` is a list at its base level with an object for each case. The attributes of each of these objects are described below.

- `case_id` (String): A unique identifier for each case. This takes the form of "case_" followed by five digits, where the least significant digits correspond to the case index and unused digits are assigned zero. For instance, "case_00000", "case_00017", "case_00202"
- `birth_year` (Integer): The year in which the patient was born. All patients born during or before 1939 are listed as simply 1939 to protect anonymity.
- `nephrectomy_year` (Integer): The year in which this patient underwent surgery for their kidney tumor or tumors.
- `gender` (Categorical): The gender of the patient. This takes one of the following values: {"male", "female"}
- `body_mass_index` (Float): The body mass index of the patient at the time measured nearest to the most recent imaging in the dataset. This takes the value of Null when it is unknown.
- `comorbidities` (Object - Bitmap): This takes an object with the following boolean attributes: `myocardial_infarction`, `congestive_heart_failure`, `peripheral_vascular_disease`, `cerebrovascular_disease`, `dementia`, `copd`, `connective_tissue_disease`, `peptic_ulcer_disease`, `uncomplicated_diabetes_mellitus`, `diabetes_mellitus_with_end_organ_damage`, `chronic_kidney_disease`, `hemiplegia_from_stroke`, `leukemia`, `malignant_lymphoma`, `localized_solid_tumor`, `metastatic_solid_tumor`, `mild_liver_disease`, `moderate_to_severe_liver_disease`, `aids`
- `surgical_history` (Object - Bitmap): This takes an object with the following boolean attributes: `cabg`, `percutaneous_coronary_artery_stenting`, `colectomy_or_proctectomy`, `solid_organ_transplant`, `nonurologic_open_abdominal_surgery`, `nonurologic_laparoscopic_surgery`, `ipsolateral_kidney_surgery`, `laproscopic_urologic_surgery`, `open_urologic_surgery`
- `selected_medications` (Object - Bitmap): This takes an object with the following boolean attributes: `antiplatelets`, `anticoagulants`, `immunosuppressive`, `hypertension`

- `smoking_history` (Categorical): This attribute can take any of the following values: {"never_smoked", "previous_smoker", "current_smoker"} or null if this is not known.
- `year_quit_smoking` (Integer): The year in which the patient quit smoking. This takes the value of null for cases in which it is not applicable.
- `pack_years` (Float): The number of cigarette pack-years that this patient has smoked. This takes the value null if it is unknown.
- `chewing_tobacco_use` (Categorical): This attribute can take any of the following values: "never_or_not_for_more_than_3mo", "quit_in_last_3mo", "currently_chews"} or null if this is not known.
- `alcohol_use` (Categorical): : This attribute can take any of the following values: "never_or_not_for_more_than_3mo", "two_or_less_daily", "more_than_two_daily", "quit_in_last_3mo"} or null if this is not known.
- `intraoperative_complications` (Object - Bitmap): This takes an object with the following boolean attributes: `blood_transfusion`, `injury_to_surrounding_organ`, `cardiac_event`
- `hospitalization` (Integer): The number of days this patient spent in the hospital after their nephrectomy operation.
- `ischemia_time` (Integer): The number of minutes that the kidney was deprived of blood during the nephrectomy operation. This takes the value of null for radical nephrectomies.
- `pathologic_size` (Float): The size of the tumor reported in the pathology report. This takes the value null when it was unable to be determined.
- `cancerous_tumor` (Categorical): "Malignant" if the post-operative surgical pathology report indicates that the tumor was indeed malignant, "Benign" if the report indicates that the tumor is benign, or "unknown" if this is unable to be determined.
- `pathology_t_stage` (Categorical): The T-stage reported in the post-operative surgical pathology report. This takes one of the following {"X", "0", "1a", "1b", "1c", "2a", "2b", "3", "4"}
- `pathology_n_stage` (Categorical): The N-stage reported in the post-operative surgical pathology report. This takes one of the following {"X", "0", "1"}
- `pathology_m_stage` (Categorical): The M-stage reported in the post-operative surgical pathology report. This takes one of the following {"X", "0", "1"}
- `tumor_histologic_subtype` (Categorical): The histologic subtype proved by either biopsy or surgical pathology. This takes one of the following values {"clear_cell_rcc", "clear_cell_papillary_rcc", "papillary", "chromophobe", "urothelial", "rcc_unclassified", "multilocular_cystic_rcc", "wilms", "oncocytoma", "angiomyolipoma", "mest", "spindle_cell_neoplasm"}.
- `tumor_necrosis` (Boolean): True if the post-operative surgical pathology report indicates that necrotic tissue is present within the tumor, False if the report indicates that it is not.
- `tumor_isup_grade` (Integer): The WHO ISUP [5] grade of the tumor indicated in the post-operative surgical pathology report. The value of Null is

used for cases where ISUP grade does not apply, such as benign tumors or Chromophobes.

- `clavien_surgical_complications` (Categorical): This takes one of following values defined by the Clavien Dindo Grade [4]: {"0", "1", "2", "3a", "3b", "4", "5"}
- `er_visit` (Boolean): True if the patient visited the ER less than 23 hours after discharge but was not admitted, false otherwise.
- `readmission` (Boolean): True if the patient was readmitted to a hospital within 90 days of the surgery, false otherwise
- `estimated_blood_loss` (Integer): The volume of blood that the surgeon estimates was lost during the nephrectomy procedure.
- `surgery_type` (Categorical): Takes one of the following values {"Open", "Laparoscopic", or "Robotic"}.
- `surgical_procedure` (Categorical): Takes one of the following values {"partial_nephrectomy", "radical_nephrectomy"}.
- `surgical_approach` (Categorical): Takes one of the following values {"retroperitoneal", "transperitoneal"}.
- `operative_time` (Integer): The time that the nephrectomy procedure took in minutes.
- `cytoreductive` (Boolean): True if the nephrectomy was performed for debulking purposes, false otherwise
- `resection_margins` (Categorical): "True" if the post-operative surgical pathology report indicates that there is malignant tissue still present in the margins of the excised tissue, "False" if the report indicates that the margins are clear.
- `preop_imaging` (Object): This is an object with the following attributes:
 - `arterial_series` ("String"): The relative location of the arterial-phase CT series blob in `data/`
 - `arterial_segmentation` ("String"): The relative location of the arterial-phase CT series' corresponding segmentation mask blob in `data/`
 - `collected_slice_thickness` (Float): The distance between captured axial sections in millimeters
 - `collected_pixel_width` (Float): The distance between centers of adjacent pixels in axial sections in millimeters

4 Technical Validation

At the time of writing this preprint, an experiment is underway to quantify the interobserver variability in recording each of the chart review attributes as well as that of the image annotations. This experiment repeats all of our quality assurance measures reported in Section 2.4.

Further, in conjunction with the release of the imaging data and segmentation masks, challenge participants were invited to review the data themselves and bring to light any issues they may find. All issues brought to light prior to April 5, 2019 will be corrected in the final training data release on April 15, 2019.

All issues discovered after April will also be corrected, but not released until after the July 29 MICCAI challenge deadline. This is to provide stability for the challenge participants and not punish those who perform their development and training before newly discovered issues are corrected.

5 Usage Notes

In addition to the release of this data, we have also released some Python starter code which includes scripts to load and visualize the data, as well as export selected portions of the data to the spreadsheet-compatible Comma Separated Values (CSV) format. At the time of writing this preprint, the imaging and semantic segmentation masks for the 210 training cases have been released at <https://github.com/neheller/kits19>. The clinical attributes within `kits.json` will be released pending further approval from our Institutional Review Board.

Acknowledgements

Research reported in this publication was supported by the National Cancer Institute of the National Institutes of Health under Award Number R01CA225435. The content is solely the responsibility of the authors and does not necessarily represent the official views of the National Institutes of Health.

We also gratefully acknowledge Climb 4 Kidney Cancer (C4KC) for providing student scholarships which were essential to the collection and annotation of this data. C4KC is an organization dedicated to advocacy for kidney cancer patients and the advancement of kidney cancer research. More information about C4KC can be found at climb4kc.org

References

1. Bray, F., Ferlay, J., Soerjomataram, I., Siegel, R.L., Torre, L.A., Jemal, A.: Global cancer statistics 2018: Globocan estimates of incidence and mortality worldwide for 36 cancers in 185 countries. *CA: a cancer journal for clinicians* **68**(6), 394–424 (2018)
2. Capitanio, U., Montorsi, F.: Renal cancer. *The Lancet* **387**(10021), 894–906 (2016)
3. Chow, W.H., Dong, L.M., Devesa, S.S.: Epidemiology and risk factors for kidney cancer. *Nature Reviews Urology* **7**(5), 245 (2010)
4. Clavien, P.A., Sanabria, J.R., Strasberg, S.M.: Proposed classification of complications of surgery with examples of utility in cholecystectomy. *Surgery* **111**(5), 518–526 (1992)
5. Epstein, J.I., Amin, M.B., Reuter, V.R., Mostofi, F.K., Committee, B.C.C., et al.: The world health organization/international society of urological pathology consensus classification of urothelial (transitional cell) neoplasms of the urinary bladder. *The American journal of surgical pathology* **22**(12), 1435–1448 (1998)
6. Ficarra, V., Novara, G., Secco, S., Macchi, V., Porzionato, A., De Caro, R., Artibani, W.: Preoperative aspects and dimensions used for an anatomical (padua) classification of renal tumours in patients who are candidates for nephron-sparing surgery. *European urology* **56**(5), 786–793 (2009)

7. Gahan, J.C., Richter, M.D., Seideman, C.A., Trimmer, C., Chan, D., Weaver, M., Olweny, E.O., Cadeddu, J.A.: The performance of a modified renal nephrometry score in predicting renal mass radiofrequency ablation success. *Urology* **85**(1), 125–129 (2015)
8. Heller, N., Dean, J., Papanikolopoulos, N.: Imperfect segmentation labels: How much do they matter? In: *Intravascular Imaging and Computer Assisted Stenting and Large-Scale Annotation of Biomedical Data and Expert Label Synthesis*, pp. 112–120. Springer (2018)
9. Heller, N., Stanitsas, P., Morellas, V., Papanikolopoulos, N.: A web-based platform for distributed annotation of computerized tomography scans. In: *Intravascular Imaging and Computer Assisted Stenting, and Large-Scale Annotation of Biomedical Data and Expert Label Synthesis*, pp. 136–145. Springer (2017)
10. Homma, Y., Kawabe, K., Kitamura, T., Nishimura, Y., Shinohara, M., Kondo, Y., Saito, I., Minowada, S., Asakage, Y.: Increased incidental detection and reduced mortality in renal cancer recent retrospective analysis at eight institutions. *International journal of urology* **2**(2), 77–80 (1995)
11. Joshi, S.S., Uzzo, R.G.: Renal tumor anatomic complexity: clinical implications for urologists. *Urologic Clinics* **44**(2), 179–187 (2017)
12. Kutikov, A., Smaldone, M.C., Egleston, B.L., Manley, B.J., Canter, D.J., Simhan, J., Boorjian, S.A., Viterbo, R., Chen, D.Y., Greenberg, R.E., et al.: Anatomic features of enhancing renal masses predict malignant and high-grade pathology: a preoperative nomogram using the renal nephrometry score. *European urology* **60**(2), 241–248 (2011)
13. Kutikov, A., Uzzo, R.G.: The renal nephrometry score: a comprehensive standardized system for quantitating renal tumor size, location and depth. *The Journal of urology* **182**(3), 844–853 (2009)
14. Lepor, H.: *Prostatic diseases*, vol. 2000. WB Saunders Company (2000)
15. Leslie, S., Gill, I.S., de Castro Abreu, A.L., Rahmanuddin, S., Gill, K.S., Nguyen, M., Berger, A.K., Goh, A.C., Cai, J., Duddalwar, V.A., et al.: Renal tumor contact surface area: a novel parameter for predicting complexity and outcomes of partial nephrectomy. *European urology* **66**(5), 884–893 (2014)
16. Lu, H., Hsiao, T., Li, X., Liang, Z.: Noise properties of low-dose ct projections and noise treatment by scale transformations. In: *2001 IEEE Nuclear Science Symposium Conference Record (Cat. No. 01CH37310)*. vol. 3, pp. 1662–1666. IEEE (2001)
17. Maxwell, A.W., Baird, G.L., Iannuccilli, J.D., Mayo-Smith, W.W., Dupuy, D.E.: Renal cell carcinoma: comparison of renal nephrometry and padua scores with maximum tumor diameter for prediction of local recurrence after thermal ablation. *Radiology* **283**(2), 590–597 (2016)
18. Osawa, T., Hafez, K.S., Miller, D.C., Montgomery, J.S., Morgan, T.M., Palapattu, G.S., Weizer, A.Z., Caoili, E.M., Ellis, J.H., Kunju, L.P., et al.: Comparison of percutaneous renal mass biopsy and renal nephrometry score nomograms for determining benign vs malignant disease and low-risk vs high-risk renal tumors. *Urology* **96**, 87–92 (2016)
19. Parkin, D.M., Bray, F., Ferlay, J., Pisani, P.: Global cancer statistics, 2002. *CA: a cancer journal for clinicians* **55**(2), 74–108 (2005)
20. Simmons, M.N., Ching, C.B., Samplaski, M.K., Park, C.H., Gill, I.S.: Kidney tumor location measurement using the c index method. *The Journal of urology* **183**(5), 1708–1713 (2010)

21. Sun, M., Abdollah, F., Bianchi, M., Trinh, Q.D., Jeldres, C., Thuret, R., Tian, Z., Shariat, S.F., Montorsi, F., Perrotte, P., et al.: Treatment management of small renal masses in the 21st century: a paradigm shift. *Annals of surgical oncology* **19**(7), 2380–2387 (2012)
22. Yap, F.Y., Hwang, D.H., Cen, S.Y., Varghese, B.A., Desai, B., Quinn, B.D., Gupta, M.N., Rajarubendra, N., Desai, M.M., Aron, M., et al.: Quantitative contour analysis as an image-based discriminator between benign and malignant renal tumors. *Urology* **114**, 121–127 (2018)